Effect of Carbon, Manganese and Chromium Concentrations, Densities, Sintering Temperatures and Post-Sintering Cooling Rates on Properties of Lean Alloy PM Steels

by

F. Chagnon[1], J. Campbell-Tremblay[1] and C. Blais[2]

[1]Rio Tinto Metal Powders
[2]Laval University

ABSTRACT

A comprehensive study has been carried out to evaluate the effect of C, Mn and Cr concentrations as well as density, sintering temperature and post-sintering cooling rate on properties of lean alloy PM steels produced with a 0.5% Mo low alloy steel and a carbon master alloy containing 2% C and 1% Si. A Taguchi L27 array was used to minimize the number of tests while getting enough data to develop predicting models.

The dimensional change increased linearly with the green density and concentrations of C, Mn and Cr and decreased with the sintering temperature. Apparent hardness increased linearly with the concentrations of C, Mn and Cr, sintered density and post-sintering cooling rate. However, tensile and yield strengths did not follow a linear model. For increased concentrations of C, Mn and Cr, maxima were shifted toward lower carbon concentrations as the levels of Mn, Cr and the post-sintering cooling rate increased. Finally, elongation increased linearly with sintered density but decreased linearly with the concentrations of C, Mn and Cr and with the post sintering-cooling rate.

INTRODUCTION

Many R&D works are currently carried out to develop new lean Ni-free PM steels. Since the use of ferroalloys is known for quite a long period of time[1-2-3-4], other production routes using master alloys are being seriously explored to improve the diffusion of the alloying elements[5-6-7-8-9-10-11-12]. Indeed, by selecting the right concentration of elements, it is possible to produce a liquid phase that when heated to the sintering temperature, promotes diffusion of the alloying elements. However, elements like manganese or chromium have a high tendency to oxidize. Therefore, furnace atmospheres with low dew

points are required to prevent oxidation of these elements. Castro and al.[13] also reported that master alloys generating liquid during sintering dissolve a significant amount of iron, which prevents oxidation of the alloying elements and facilitate their diffusion in the iron matrix. However, low dew point atmospheres are still recommended to correctly sinter these materials.

In a previous study[14], a new approach combining the use of low alloy steel powders admixed ferroalloys and a carbon master alloy that was produced from water atomization of a high carbon melt containing 1% Si was evaluated with promising results and recommendations were made to further characterize these materials.

Therefore, the objective of this study is to characterize the effect of carbon, manganese and chromium concentrations as well as density, sintering temperature and post-sintering-cooling rate on properties of lean alloy PM steels produced with a 0.5% Mo low alloy steel powder with additions of carbon master alloy, ferromanganese and ferrochromium to adjust the carbon, Mn and Cr concentrations in the materials.

EXPERIMENTAL PROCEDURE

The base powders used in this study were ATOMET 4001, a 0.5% Mo low alloy steel powder, and a carbon master alloy (M.A.) produced by water atomization of a Fe-2%C-1%Si melt. This powder was subsequently made malleable by a heat treatment, which is described more precisely in a previous paper[15]. The chemical and physical properties of these powders are given in Table 1.

Table 1. Chemical and physical properties of ATOMET 4001 and carbon master alloy.

Powder grade	Mo, %	Mn, %	Si, %	C, %	O, %	+100 mesh, %	-100/+325 mesh, %	-325 mesh, %	Apparent density, g/cm³	Flow, s/50g
ATOMET 4001	0.50	0.14	-	0.004	0.09	12	66	22	2.95	25
Carbon M.A.	-	-	1.05	1.98	0.10	12	64	24	2.85	27

A L27 Taguchi array was used to evaluate the effect of carbon, manganese and chromium concentrations as well as green densities, sintering temperatures and post-sintering cooling rates. Mixes were prepared with ferromanganese and ferrochromium to reach nominal values 0.50, 0.85 and 1.20% Mn, and 0.25, 0.40 and 0.55% Cr. The carbon concentration was varied from of 0.35 to 0.55 and 0.75% C by changing the proportion of carbon master alloy in the mix. It is worth noting that the nominal concentration of Mo decreased from about 0.40% for the lowest proportion of carbon master alloy to 0.30% for the highest one. Inversely, the silicon concentration increased from about 0.2% to 0.4 for the lowest and highest concentrations of carbon master alloy. All the mixes contained 0.75% wax as lubricant.

TRS and dog bones specimens were pressed to green densities of respectively 6.75, 6.90 and 7.05 g/cm³ and were sintered in a mesh belt furnace at either 1120, 1170 or 1200°C in a 90% nitrogen/10% hydrogen atmosphere. The post-sintering cooling rates in the range of 615 to 350°C were respectively of 1.7, 2.2 and 3.0°C/s. Figure 1 illustrates a typical sintering profile.

Table 2 summarizes the L27 Taguchi array that was used to evaluate the effect of the various variables on green and sintered properties.

Dimensional change, apparent hardness and tensile properties were determined for each test condition after tempering 60 minutes in air at 200°C. The carbon concentration after sintering was determined by

Leco analysis while the concentration of Mn and Cr were evaluated by ICP. Finally, a microstructural characterization was performed by optical microscopy.

Table 2. Taguchi L27 array used in this study.

| Trial #	Mo steel powder, %	Carbon M.A., %	C target, %	Mn target, %	Cr target , %	Temperature, °C	Cooling rate, °C/s	Green density, g/cm³
1	81.82	17.36	0.35	0.50	0.25	1120	3.0	6.75
2	71.88	27.26	0.55	0.50	0.25	1170	2.2	6.90
3	61.95	37.17	0.75	0.50	0.25	1200	1.7	7.05
4	81.55	17.30	0.35	0.50	0.40	1170	1.7	7.05
5	71.64	27.17	0.55	0.50	0.40	1200	3.0	6.75
6	61.74	37.05	0.75	0.50	0.40	1120	2.2	6.90
7	81.28	17.24	0.35	0.50	0.55	1200	2.2	6.90
8	71.40	27.08	0.55	0.50	0.55	1120	1.7	7.05
9	61.54	36.92	0.75	0.50	0.55	1170	3.0	6.75
10	81.38	17.26	0.35	0.85	0.25	1200	1.7	6.90
11	71.50	27.12	0.55	0.85	0.25	1120	3.0	7.05
12	61.62	36.97	0.75	0.85	0.25	1170	2.2	6.75
13	81.11	17.21	0.35	0.85	0.40	1120	2.2	6.75
14	71.26	27.03	0.55	0.85	0.40	1170	1.7	6.90
15	61.41	36.85	0.75	0.85	0.40	1200	3.0	7.05
16	80.84	17.15	0.35	0.85	0.55	1170	3.0	7.05
17	71.02	26.94	0.55	0.85	0.55	1200	2.2	6.75
18	61.21	36.72	0.75	0.85	0.55	1120	1.7	6.90
19	80.95	17.17	0.35	1.20	0.25	1170	2.2	7.05
20	71.12	26.98	0.55	1.20	0.25	1200	1.7	6.75
21	61.29	36.77	0.75	1.20	0.25	1120	3.0	6.90
22	80.68	17.11	0.35	1.20	0.40	1200	3.0	6.90
23	70.88	26.89	0.55	1.20	0.40	1120	2.2	7.05
24	61.08	36.65	0.75	1.20	0.40	1170	1.7	6.75
25	80.41	17.06	0.35	1.20	0.55	1120	1.7	6.75
26	70.64	26.79	0.55	1.20	0.55	1170	3.0	6.90
27	60.88	36.53	0.75	1.20	0.55	1200	2.2	7.05
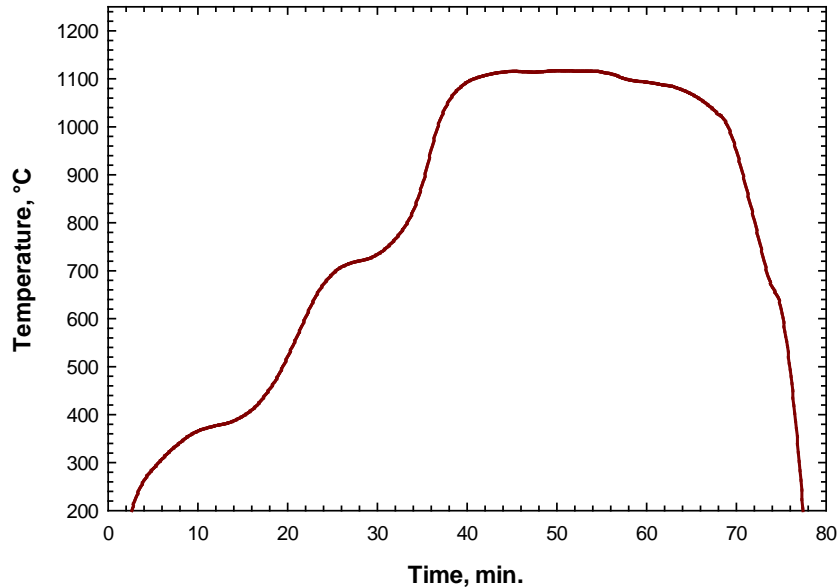
Figure 1. Typical sintering temperature profile used in this study.

RESULTS

Table 3 summarizes the compacting pressures required to reach the green density targets, as well as the chemical and sintered properties for the 27 trials. Figure 2 illustrates the mean effect of carbon, manganese and chromium concentrations as well as the green density and sintering parameters on the compacting pressure values required to reach the green density targets. The interactions graph is also illustrated. As expected the mean compacting pressure increases almost linearly with the green density but is also affected, to a lower extent, by the carbon concentration. The latter is explained by the use of an increased proportion of carbon master alloy, less compressible than the steel powder, as the sintered carbon concentration increased[14]. The relation is better illustrated in Figure 3. Green density increases with the compacting pressure but decreases when the proportion of carbon master alloy in the mix increases and the effect is amplified at highest green densities.

Figure 4 illustrates the mean effects of the carbon, manganese and chromium concentrations and green density, sintering temperature and post-sintering cooling rate on the average dimensional change of TRS specimens. The growth of the TRS specimens increases with the manganese and chromium concentrations and with the green density and to a lower extent with the carbon concentration while it decreases with the sintering temperature. No significant interaction is found between dimensional change and the chemical composition. All the relations follow a linear model and dimensional change can be predicted from the following equation:

Equation 1: DC (%) = -0.654 + 0.243 X %Mn + 0.364 X %Cr + 0.355 X (gr. dens., g/cm³) + 0.163 X %C – 0.0017 X (Temp., °C)

From this equation variations of 0.1% of Mn, Cr and C induce variations of the dimensional change of respectively of 0.024, 0.364 and 0.016%, while variations of the green density of 0.05 g/cm³ and 10°C of the sintering temperature induce variations of respectively 0.018 and 0.017%. Figure 5 illustrates the evolution of the actual dimensional change values for the 27 trials compared to the values predicted by

the linear model. The differences between the actual and predicted values are generally inferior to ±0.03% for the overall ranges of the variables.

Table 3. Green, chemical and sintered properties of the 27 trials of the Taguchi L27 array (after tempering 60 minutes at 200°C).

| Test #	Green density, g/cm³	Temp., °C	Cooling Rate, °C/s	Comp. press., MPa	Mn, %	Cr, %	C, %	Dim. change, % vs die size	Sintered density, g/cm³	App. hard., HRA	T.S., MPa	Y.S., MPa	Elong., %
1	6.75	1120	3.0	440	0.47	0.19	0.36	0.12	6.73	39	406	315	1.8
2	6.90	1170	2.2	539	0.48	0.23	0.50	0.08	6.89	48	586	439	1.9
3	7.05	1200	1.7	709	0.50	0.26	0.70	0.11	7.07	56	801	584	0.8
4	7.05	1170	1.7	612	0.49	0.40	0.34	0.17	7.04	48	574	433	2.8
5	6.75	1200	3.0	468	0.49	0.44	0.53	0.05	6.75	51	634	476	1.5
6	6.90	1120	2.2	577	0.49	0.28	0.77	0.25	6.87	57	680	526	1.1
7	6.90	1200	2.2	516	0.49	0.60	0.36	0.12	6.89	47	562	419	2.0
8	7.05	1120	1.7	659	0.49	0.40	0.60	0.29	7.02	52	659	490	1.6
9	6.75	1170	3.0	490	0.50	0.56	0.79	0.20	6.73	62	673	606	0.3
10	6.90	1200	1.7	516	0.84	0.25	0.34	0.09	6.90	46	539	405	2.4
11	7.05	1120	3.0	659	0.85	0.19	0.58	0.29	7.02	58	727	556	1.3
12	6.75	1170	2.2	490	0.85	0.24	0.76	0.17	6.74	63	658	586	0.3
13	6.75	1120	2.2	447	0.84	0.31	0.41	0.20	6.72	49	552	419	1.4
14	6.90	1170	1.7	546	0.85	0.39	0.57	0.24	6.87	57	744	556	1.1
15	7.05	1200	3.0	720	0.86	0.45	0.73	0.32	7.02	70	831	721	0.3
16	7.05	1170	3.0	623	0.86	0.58	0.38	0.33	7.01	59	784	570	1.5
17	6.75	1200	2.2	474	0.84	0.63	0.59	0.23	6.71	60	757	608	0.6
18	6.90	1120	1.7	585	0.88	0.41	0.82	0.38	6.84	61	679	567	0.5
19	7.05	1170	2.2	625	1.23	0.24	0.38	0.31	7.01	58	784	581	1.5
20	6.75	1200	1.7	470	1.24	0.26	0.56	0.18	6.72	57	716	619	0.5
21	6.90	1120	3.0	585	1.26	0.20	0.81	0.39	6.85	66	628	559	0.3
22	6.90	1200	3.0	523	1.21	0.45	0.37	0.28	6.85	59	782	581	1.2
23	7.05	1120	2.2	676	1.22	0.32	0.65	0.45	6.99	65	799	673	0.5
24	6.75	1170	1.7	497	1.26	0.43	0.80	0.31	6.70	65	574	554	0.2
25	6.75	1120	1.7	452	1.19	0.45	0.45	0.35	6.69	56	663	542	0.7
26	6.90	1170	3.0	556	1.24	0.58	0.61	0.42	6.83	66	669	600	0.2
27	7.05	1200	2.2	739	1.22	0.64	0.78	0.48	6.99	70	723	619	0.3
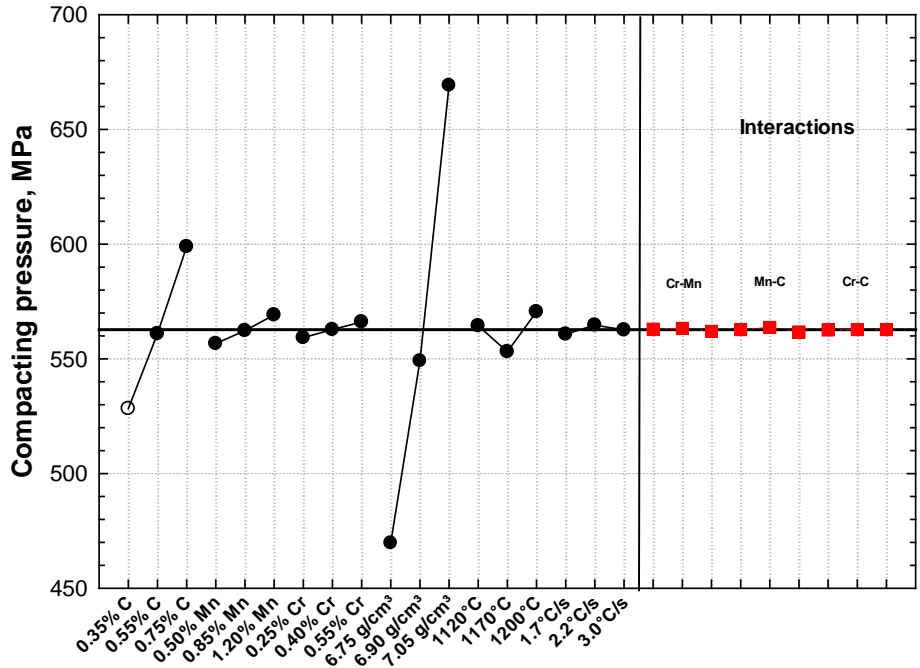
Figure 2. Mean effects of carbon, manganese and chromium concentrations, green density, sintering temperature and post-sintering cooling rate on the compacting pressure required to reach the green density targets.
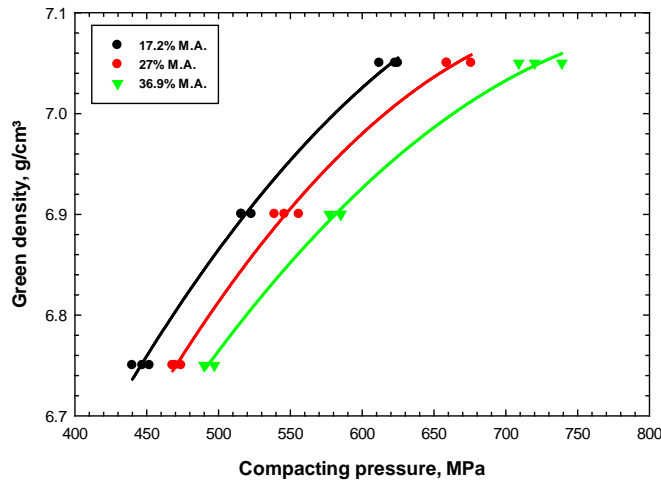

Figure 3. Variation of green density with compacting pressure and the proportion of carbon master alloy in the mixes.

Figure 6 illustrates the mean effects of the carbon, manganese and chromium concentrations and green density, sintering temperature and post-sintering cooling rate on sintered density of the TRS specimens. The sintered density is proportional to the green density and all the other parameters play a minor role for this property and no significant interaction is found with the chemical elements.
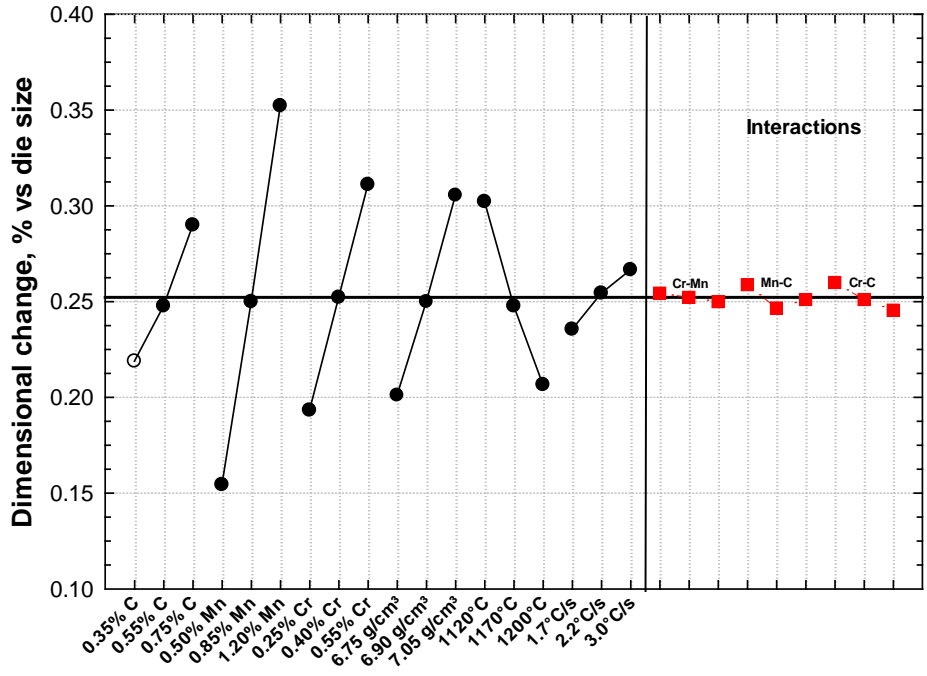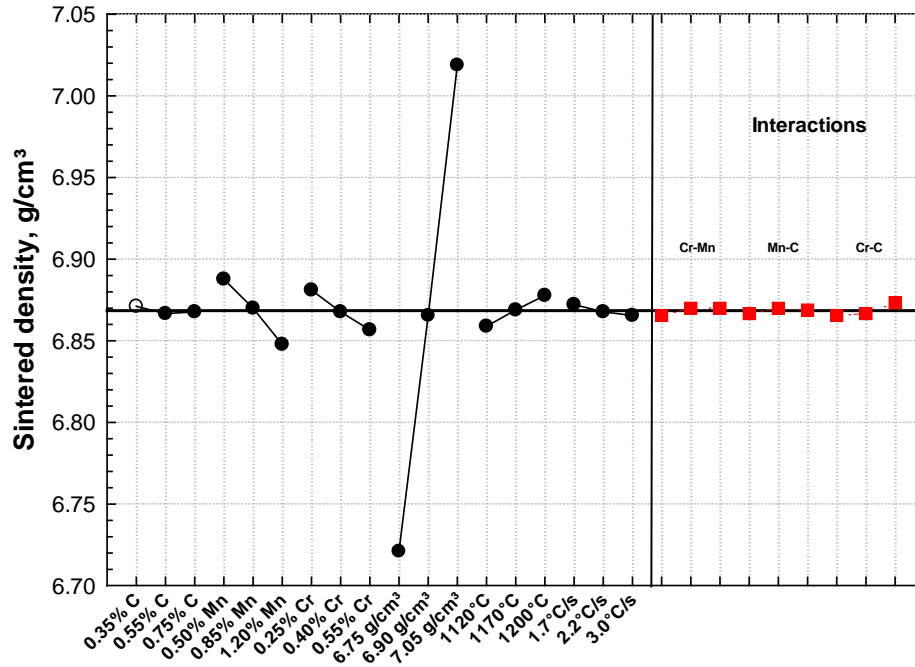
Figure 4. Mean effects of carbon, manganese and chromium concentrations, green density, sintering temperature and post-sintering cooling rate on dimensional change of TRS specimens produced with the various mixes.
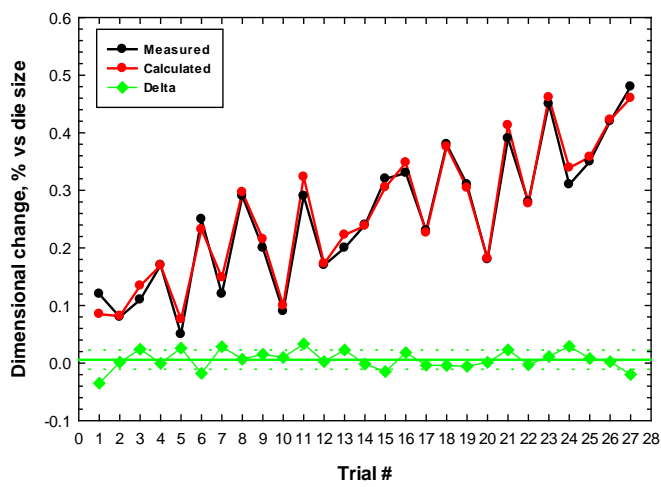
Figure 5. Actual dimensional change values measured for the 27 trials vs those predicted by the linear model.

Figure 7 illustrates the mean effects of the carbon, manganese and chromium concentrations and green density, sintering temperature and post-sintering cooling rate on the apparent hardness of TRS specimens. Apparent hardness is mainly affected by the carbon and manganese concentrations and to a lower extent by the chromium concentration, green density and post-sintering cooling rate. The interactions graph shows some minor interaction but based on the mean effect results, the relations seem to follow a linear model with the following equation:

Equation 2: App. Hard. (HRA) =   **-80.3 + 29.4 X %C + 13.5 X %Mn + 13.6 * %Cr + 14 X (sint. dens., g/cm³) + 2.3 X (cooling rate, °C/s)**

8

From this model, a variation of 0.1% of the carbon, manganese and chromium concentrations induces a variation of apparent hardness of respectively 2.9, 1.4 and 1.4 HRA, while variations of sintered density of 0.1 g/cm³ and 1°C/s of the cooling rate induce an apparent hardness variation of respectively 1.4 and 2.3 HRA. Figure 8 illustrates the actual apparent hardness values measured for the 27 trials compared to those predicted by the model. For the 27 trials, the model predicts apparent hardness with an accuracy of ±2 HRA in about 85% of the time.

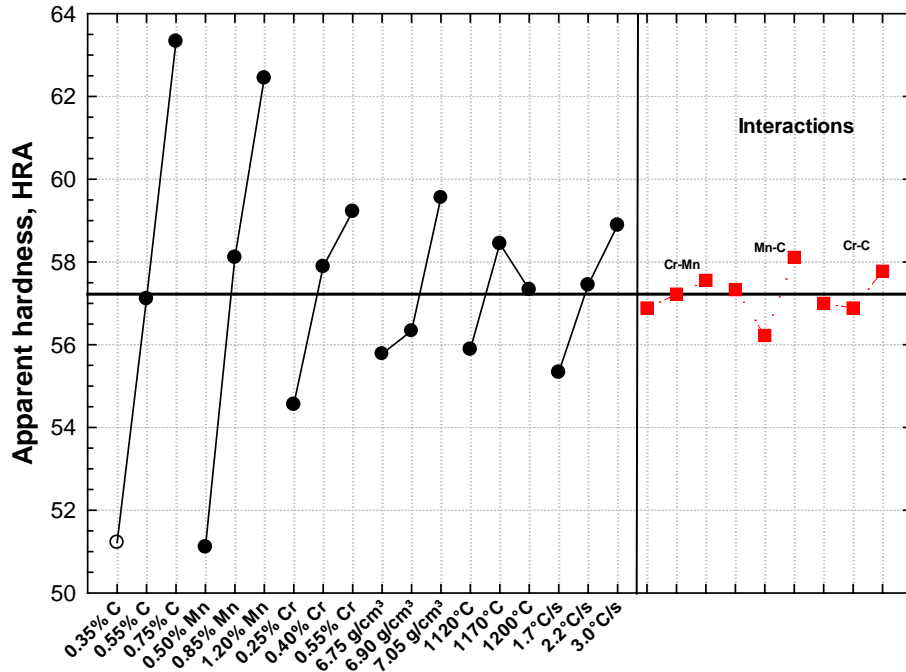**Figure 6. Mean effects of carbon, manganese and chromium concentrations, green density, sintering temperature and post-sintering cooling rate on sintered density of TRS specimens produced with the various mixes.**

Figure 9 illustrates the mean effects of the carbon, manganese and chromium concentrations and green density, sintering temperature and post-sintering cooling rate on the tensile strength. Tensile strength is mainly affected by the density, the carbon, manganese and chromium concentrations, sintering temperature and to a lower extent by the post-sintering cooling rate. However, on the interactions graph, significant interactions occur with the chemical elements particularly with carbon. From previous studies on sinterhardened PM steels[16-17-18], tensile strength increased with carbon concentration to reach a maximum and then decreased. The maxima observed were generally shifted toward lower carbon concentrations as the material hardenability and post-cooling rate increased. Therefore, this property would not follow a fully linear model, depending of the alloy composition and post-sintering cooling rate. In order to develop a valuable model, the ascending part of the curve was developed by an iteration process. Multiple linear regression analyses were made by removing tensile strength values exceeding 50 MPa the predicted values until the model can predict all the values within ±50 MPa. At the end of the iteration process, the ascending portion of the curve can be predicted by the following equation:

Equation 3: T.S. (MPa) = -3710 + 441 X (sint. dens., g/cm³) + 576 X %C + 280 X %Mn + 255 X %Cr + 0.575 X (temp., °C) + 38 X (C.R., °C/s)

9

Figure 7. Mean effects of carbon, manganese and chromium concentrations, green density, sintering temperature and post-sintering cooling rate on apparent hardness of TRS specimens produced with the various mixes.
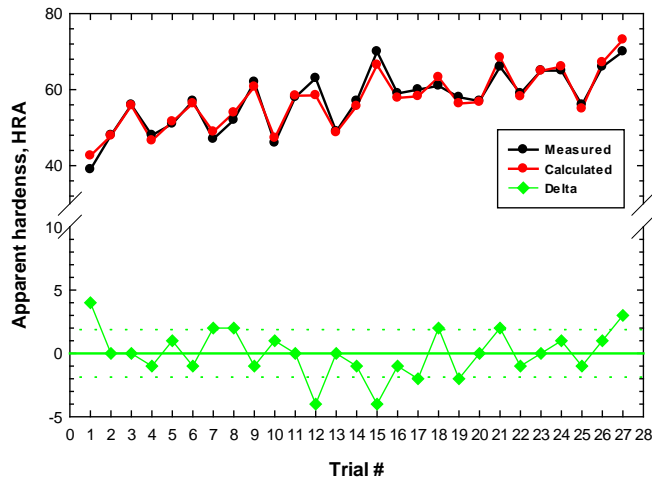

Figure 8. Actual apparent hardness values measured for the 27 trials vs those predicted by the linear model.

This model is not valid for a combination of the following conditions:

- Cooling rate ≥ 2.5°C, %C ≥ 0.7, %Mn ≥ 0.5 et %Cr≥ 0.5 or
- Cooling rate ≥ 1.6°C, %C ≥ 0.7, %Mn ≥ 0.85 et %Cr≥ 0.4 or
- Cooling rate ≥ 1.9°C, %C ≥ 0.6, %Mn ≥ 0.85 et %Cr≥ 0.19.

To predict descending portion of the curve, the differences between the measured and predicted values for the above conditions was then calculated by a second multiple linear regression analysis to get the following equation:

Equation 4:   **Delta T.S. (MPa) = -1283 + 1026 X %C + 416 X %Mn + 368 X %Cr +55 X (C.R., °C/s)**

Both portions of the curves are then joined together by a polynomial regression. Figure 10 illustrates an example of estimation of tensile strength with the carbon concentration for %Mn of 0.7, %Cr of 0.5, sintering temperature of 1170°C, post-cooling rate of 3°C/s and sintered density of 6.9 g/cm³. Figure 11 illustrates similar estimations as a function of the carbon concentration for concentrations of manganese of respectively 0.50 and 0.75%, chromium concentrations of respectively 0.25 and 0.5%, sintering temperature of 1170°C, post-sintering cooling rate of 2°C/s and sintered density of 7.0 g/cm³. As expected, maxima are shifted towards lower carbon concentrations as the concentrations of Mn and Cr increase.

Figure 12 illustrates the actual tensile strength values measured for the 27 trials compared to the values predicted by the model. For the 27 trials, the model predict tensile strength values at ± 30 MPa in about 80% of the time.
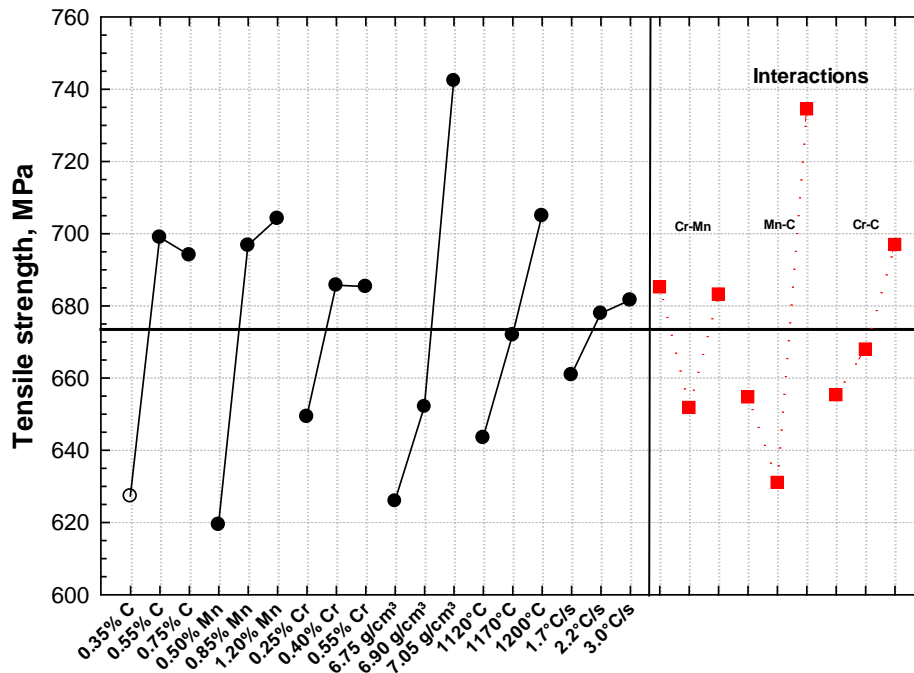

Figure 9. Mean effects of carbon, manganese and chromium concentrations, green density, sintering temperature and post-sintering cooling rate on tensile strength of dog bone specimens produced with the various mixes.

Figure 13 illustrates the mean effects of the carbon, manganese and chromium concentrations and green density, sintering temperature and post-sintering cooling rate on the yield strength. Yield strength is mainly affected by the carbon and manganese concentrations and to a lower extent by the density, chromium concentration, sintering temperature and the post-sintering cooling rate. However, as for tensile strength, there are significant interactions between the chemical elements suggesting this variable does not follow a linear model.
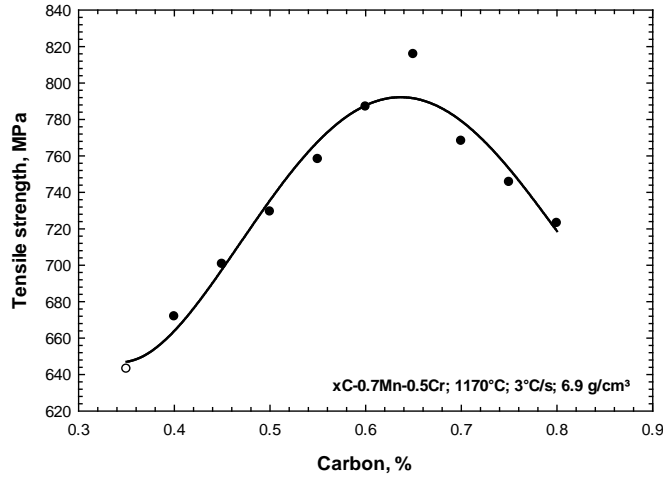
11

Figure 10. Example of estimation of tensile strength from Equation 3 and Equation 4.
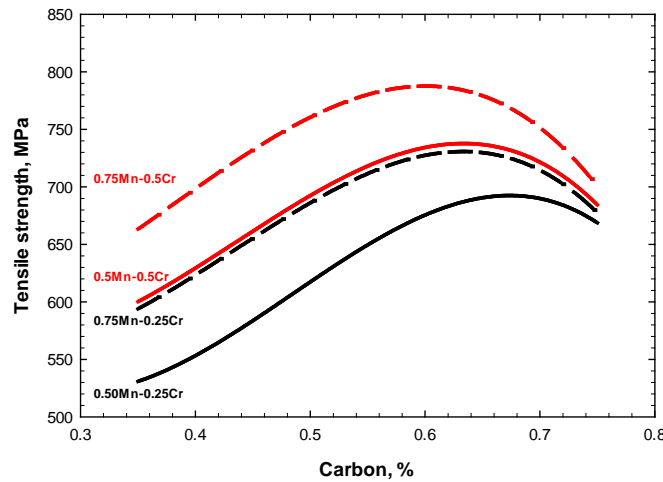

Figure 11. Estimation of tensile strength with carbon concentration for a sintering temperature of 1170°C and a post-sintering cooling rate of 2°C/s and a density of 7.0 g/cm³.
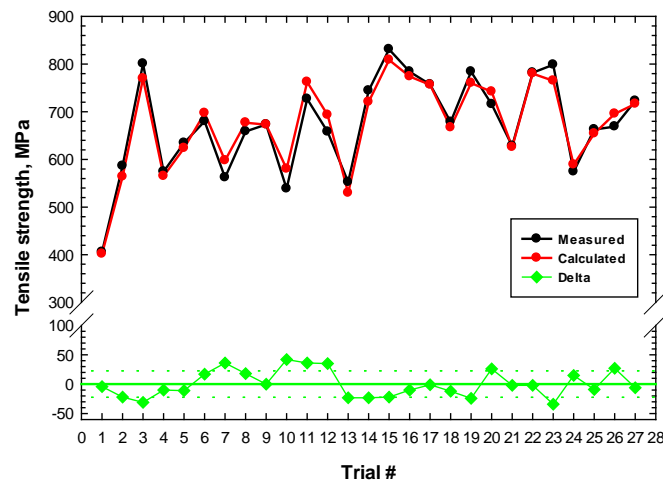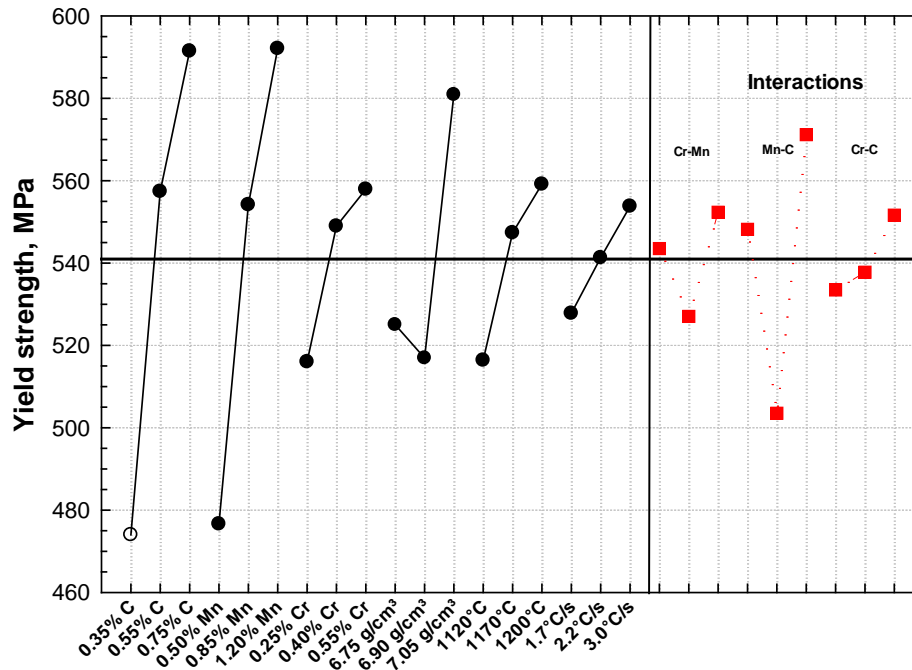

Figure 12. Actual tensile strength values measured for the 27 trials vs those predicted by the model.

Figure 13. Mean effects of carbon, manganese and chromium concentrations, green density, sintering temperature and post-sintering cooling rate on yield strength of dog bone specimens produced with the various mixes.

Therefore the same procedure was applied as for the tensile strength to develop a model to predict yield strength. The ascending portion of the curve can be predicted by the following equation:

Equation 5: Y.S. (MPa) = -2032 + 466 X %C + 232 X %Mn + 186 X %Cr + 220 X (sint. dens., g/cm³) 0.441 X (temp., °C) + 18 X (C.R., °C/s)

This model is not valid for a combination of the following conditions:

- Cooling rate ≥ 1.7°C, %C ≥ 0.75, %Mn ≥ 0.85 et %Cr ≥ 0.4 or
- Cooling rate ≥ 3.0°C, %C ≥ 0.6, %Mn ≥ 1.2 et %Cr ≥ 0.2.

As for tensile strength, in order to predict descending portion of the curve, the differences between the measured yield strength values and predicted values for the above conditions were then calculated by a second multiple linear regression analysis to get the following equation:

Equation 6: Delta Y.S. (MPa) = -879 + 672 X %C + 255 X % Mn + 228 X %Cr + 42 X (C.R., °C/s)

Examples of estimation of yield strength as a function of carbon concentration with manganese concentrations of respectively 0.5 and 1%, chromium concentrations of respectively 0.25 and 0.5% for a sintering temperature of 1170°C, post-sintering cooling rate of 2°C/s and sintered density of 7.0 g/cm³ are illustrated in Figure 14. Within 0.35 to 0.7% C, for these conditions, yield strength increases linearly with carbon, Mn and Cr concentrations, except at 1% Mn and 0.5% Cr where a maximum is reached at about 0.65%, 650 MPa, and then decreases for carbon concentrations higher than 0.65%.

13

Figure 15 illustrates the actual yield strength values measured for the 27 trials compared to the values predicted by the model. For the 27 trials, the model predicts yield strength values at ± 30 MPa in about 90% of the time.
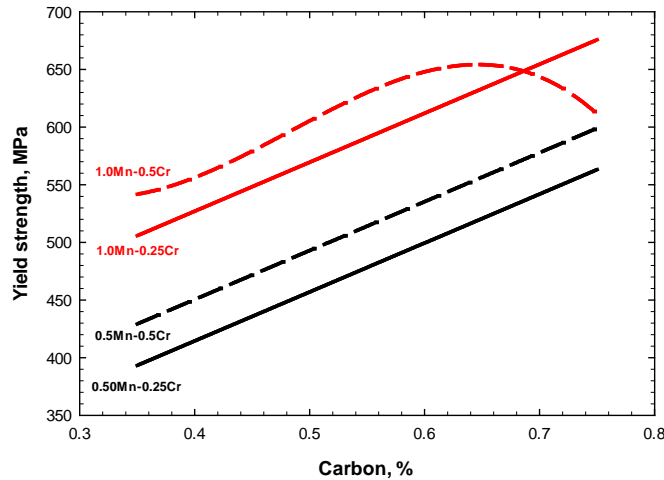

Figure 14. Estimation of yield strength with carbon concentration for a sintering temperature of 1170°C and a post-sintering cooling rate of 2°C/s and a density of 7.0 g/cm³..
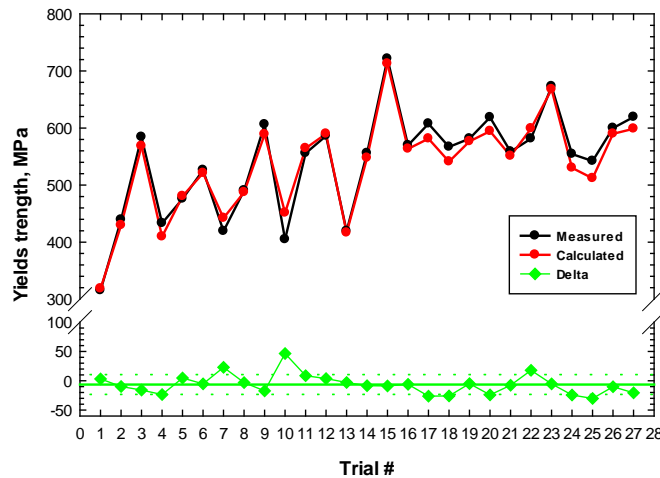

Figure 15. Actual yield strength values measured for the 27 trials vs those predicted by the model.

Figure 16 illustrates the mean effects of the carbon, manganese and chromium concentrations and green density, sintering temperature and post-sintering cooling rate on elongation. Elongation is mainly affected by the carbon and manganese concentrations and to a lower extent by the chromium concentration, post-sintering cooling rate and sintering temperature. Elongation decreases when the concentrations of C, Mn, Cr and with the post-sintering cooling rate while it increases with the sintered density. As shown on the interactions graph, the interactions between the alloying elements are low and the relation with the various parameters seems to follow a linear model within their ranges of variation. Therefore, this variable can be predicted by the following equation:

Equation 7:   Elong. (%) = -3.157 - 0.96 X %Mn – 0.621 X %Cr – 3.066 X %C + 1.081 * (sint. Dens., g/cm³) – 0.166 X (C.R., °C/s)

14

From this equation, a variation of 0.1% in C, Mn and Cr will induce a variation of respectively 0.3, 0.1, 0.1%. A variation of 1°C/s and 0.1 g/cm³ will induce a variation of respectively 0.2% and 0.1%. Figure 17 illustrates the actual elongation values measured for the 27 trials compared to the values predicted by the model. For the 27 trials, the model predicts tensile strength values at ± 0.3% MPa in about 85% of the time.
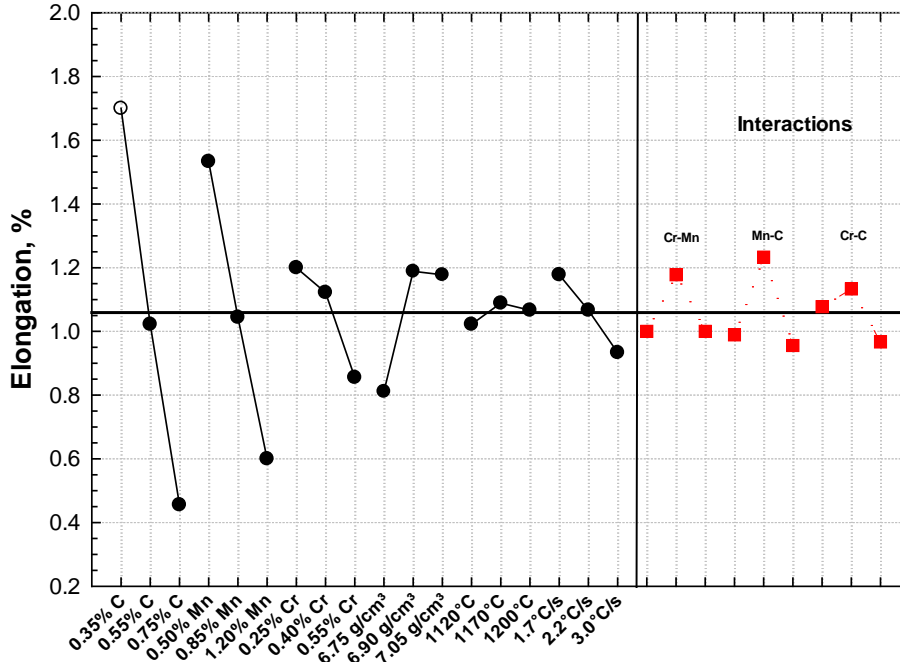

Figure 16. Mean effects of carbon, manganese and chromium concentrations, green density, sintering temperature and post-sintering cooling rate on elongation of dog bone specimens produced with the various mixes.
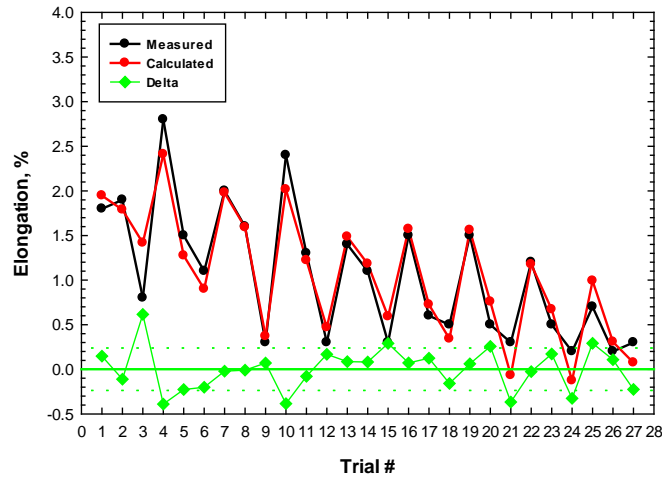

Figure 17. Actual elongation values measured for the 27 trials vs those predicted by the model.

Figure 18 shows typical microstructures of some materials with various concentrations of carbon, Mn and Cr. At low carbon concentrations, the microstructure is bainitic in the 0.5% Mo steel matrix and is composed of pearlite and ferrite in the carbon master alloy particles. Some bainite can also be observed at the periphery of the carbon master alloy particles. As the carbon concentration increases, the

15

microstructure gradually shows a larger proportion of martensite with bainite or fine pearlite in the carbon master alloy. As the concentration of Mn and Cr increases, the amount of martensite increases due to the improved hardenability. It is however worth noting that some ferroalloy particles, FeCr, are visible, particularly at higher chromium concentration. This indicates this element does not diffuse completely in the steel particles.
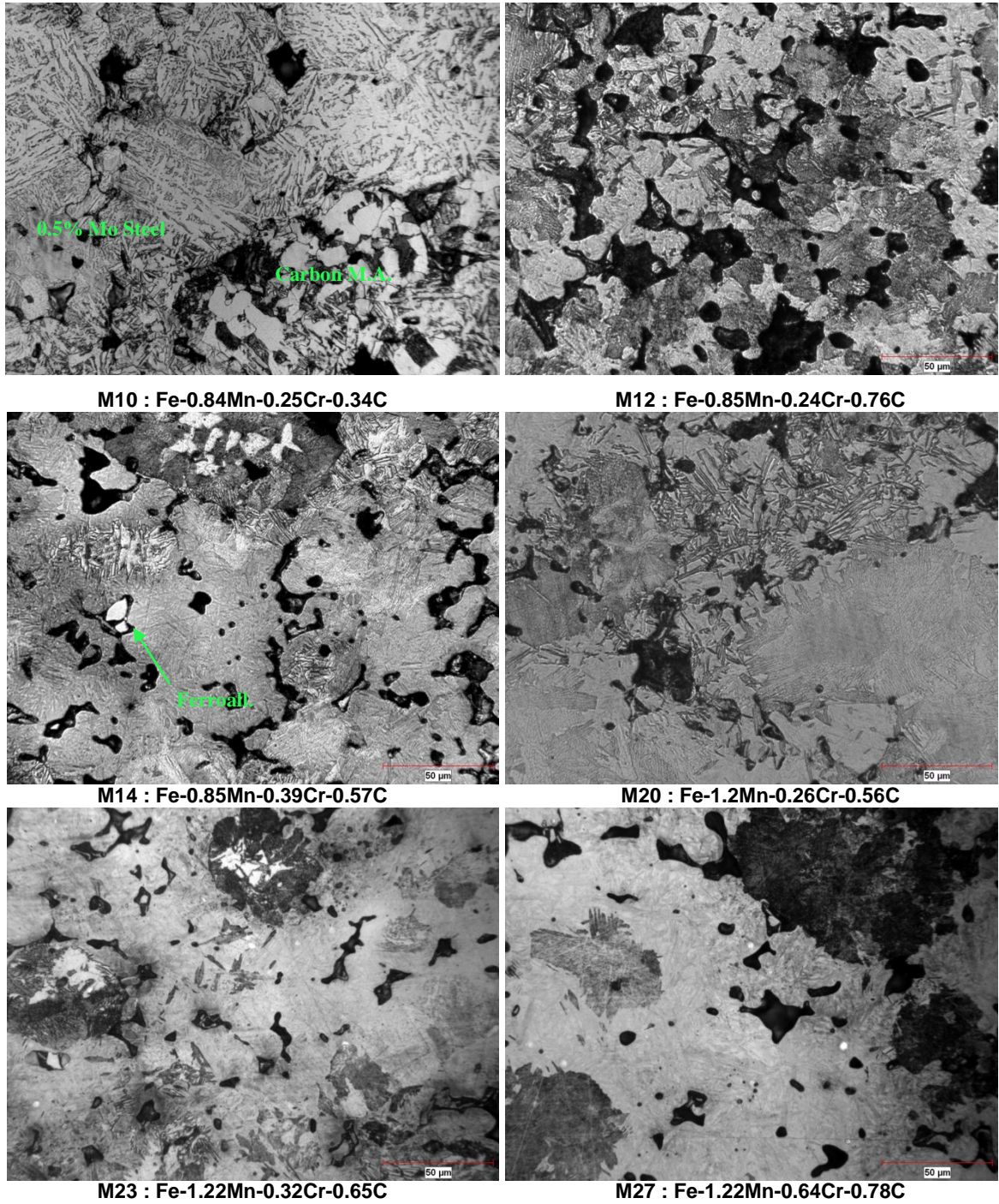

M10 : Fe-0.84Mn-0.25Cr-0.34C   **M12 : Fe-0.85Mn-0.24Cr-0.76C**

M14 : Fe-0.85Mn-0.39Cr-0.57C   **M20 : Fe-1.2Mn-0.26Cr-0.56C**

M23 : Fe-1.22Mn-0.32Cr-0.65C   **M27 : Fe-1.22Mn-0.64Cr-0.78C**

Figure 18. Typical microstructures observed after sintering Fe-Mn-Cr-C materials (Nital etching, 500X).

16

CONCLUSIONS

A comprehensive study was carried out to evaluate the effect of carbon, manganese and chromium concentrations as well as density, sintering temperature and post-sintering cooling rate on properties of lean alloy PM steels produced with a 0.5% Mo low alloy steel mixed with a carbon master alloy and ferromanganese and ferrochromium. Within the range of the various parameters used in this study:

1. The growth during sintering increased linearly with green density, concentrations of C, Mn and Cr and decreased with sintering temperature.
2. Apparent hardness increased linearly with the concentrations of C, Mn et Cr, sintered density and post-sintering cooling rate.
3. Tensile and yield strengths, did not follow a fully linear model. For increased concentrations of C, Mn and Cr, maxima were shifted toward lower carbon concentrations as the levels of Mn, Cr and the post-sintering cooling rate increased.
4. Elongation increased linearly with sintered density but decreased linearly with the concentrations of C, Mn and Cr and with the post-sintering cooling rate.

REFERENCES

[1] Shivanath, R. and Jones, P.; US Patent 5,476,632, December 19, 1995.

[2] Shivanath, R. and Jones, P.; US Patent 5,834,640, November 10, 1998.

[3] Causton, R.J.; US Patent 5,217,683, June 8, 1993.

[4] Causton, R.J.; US Patent 5,108,493, April 28, 1992.

[5] Lindsey, B., King, P and Schade, C.T.; US Patent 7,153,339, December 26, 2006.

[6] Lindsey, B., King, P and Schade, C.T.; US Patent 7,527,667, May 5, 2009.

[7] Christopherson, D.B., Farthing, L.J., Schoenwetter, T., L'Espérance, G., Beaulieu, G.; Patent Application Publication US 2009/0252636, October 8, 2009

[8] Oro, R., Campos, M., Torralba, J.M. and Capdevila, C.; "Lean Steels in PM through the use of Mn-Si Master Alloy: Alloy Design and Sintering Performance", PM2012 World Congress & Exhibition, Yokohama, JPMA, 2012.

[9] Oro, R., Torralba, J.M. and Campos, M.; "Mechanical Properties of Mn-Si Low Alloy Sintered Steels Prepared Through the Master Alloy Route", PM2012 World Congress & Exhibition, Yokohama, JPMA, 2012.

[10] Veiga, A. and Castro, F.; " Master Alloys for High Strength PM Steels"; PM2012 World Congress & Exhibition, Yokohama, JPMA, 2012.

[11] Miyake, T., Matsumoto, N. and Kondoh, M., "Influence of Densification Processes on Microstructure and Mechanical Properties of Fe-Mn-Si-C Steels"; PM2012 World Congress & Exhibition, Yokohama, JPMA, 2012.

[12] Castro, F., Sainz, S., Viega, A. and Ortiz., P.; "The Master Alloy Concept and its Consequences", PM2012 World Congress & Exhibition, Yokohama, JPMA, 2012.

[13] Castro, F., Sarasola, M., Baumgaertner, F., Dougan, M. Mitchell, S., Lipp, K., Bender, H.J., Coffin., C., Dunkley, J.; "Alloying and Sintering Behaviour of Selected Iron-Graphite-Master Alloy Powder Mixtures", EURO PM 2005, EPMA, , Shrewsbury, 2005, vol. ,1 p. 371-378.

[14] Chagnon, F and Aguirre, L.; "A New Approach to Lean Alloy PM Steels", Advabces in Powder Metallurgy & Particulate Materials, MPIF, Princeton, 2013, pp 10-78 to 10-87..

[15] Chagnon, F., Coscia, C.; "Development and Properties of a New Malleable Iron Powder Grade"; Advances in Powder Metallurgy & Particulate Materials, MPIF, Princeton, 2012, pp 10-7 to 10-20.

[16] Chagnon, F. and Gagné, M.; "Effect of Graphite And Copper Concentrations and Post Sintering Cooling Rate on Properties of Sinter Hardened Materials", Advances in Powder Metallurgy & Particulate Materials, MPIF, Princeton, 2000, part 13, pp 35-45.

[17] Chagnon, F., Olschewski, G and St-Laurent, S; "Effects of Product and Process Parameters on Dimensional Stability of Sinter Hardened Materials", EURO PM2001, Vol. 4, EPMA, Shrewsbury, 2001, pp 230-235.

[18] Chagnon. F. and Trudel, Y.: "Effect of Copper Additions on Properties of 1.5% Mo Sintered Steels", Advances in Powder Metallurgy & Particulate Materials, MPIF, Princeton, 2002, part 13, pp 73-82.